Preprints of the 21st IFAC World Congress (Virtual)
Berlin, Germany, July 12-17, 2020

Integral Resonance Control In Continuous Wave Superconducting Particle Accelerators

A. Bellandi * **J. Branlard** * **A. Eichler** * **S. Pfeiffer** *

* *Deutsches Elektronen-Synchrotron (DESY), Hamburg 22607 Germany*
(andrea.bellandi@desy.de, julien.branlard@desy.de, annika.eichler@desy.de, sven.pfeiffer@desy.de)

Abstract: Superconducting accelerating cavities for continuous wave low-current particle accelerators requires a tight resonance control to optimize the RF power costs and to minimize the beam delivery downtime. When the detuning produced by radiation pressure becomes comparable to the RF bandwidth, the monotonic instability starts to affect the cavity operation. When this instability is triggered by external vibrations or drifts, the accelerating field amplitude drops rapidly, and the beam acceleration has to be stopped. Past experiments showed that using an integral control of the piezoelectric tuners installed on the cavity prevents the adverse effects of the monotonic instability. This paper derives theoretically why an integral controller is an effective way to counteract the monotonic instability. To perform the study a linearized state-space model of the cavity is derived. Simulations and experiments in a superconducting test facility indicate that the use of this kind of control has the additional benefit of bringing the cavities to the resonance condition automatically.

Keywords: Particle accelerators, Control systems, Parametric resonances, Electromagnetic devices

1. INTRODUCTION

Superconducting Radio-Frequency (SRF) Continuous Wave (CW) electron linear accelerators are increasingly interesting for their scientific and industrial applications ranging from X-ray and UV laser generation for experimental and medical uses (Sekutowicz et al. (2015); Zhu et al. (2017); Raubenheimer (2018); Serafini et al. (2019)), short-lived isotope production for medicine and industry (Habs and Köster (2011)), and semiconductor lithography (Nakamura et al. (2015)). The main components of this kind of machines are the superconducting resonant RF cavities. When an electron bunch passes through an RF cavity, it gets accelerated by the inner electric field, thus absorbing part of the stored electromagnetic energy. To maximize the RF efficiency accelerating cavities are driven at or near the resonance frequency of the accelerating mode. Superconducting cavities possess an RF surface resistance of a factor 10^5 lower compared to their normal conducting counterparts. Therefore, they can operate continuously at fields over $10\,\mathrm{MV\,m^{-1}}$ without enduring a mechanically damaging thermal dissipation or needing excessive RF power expenditures. Cryogenic temperatures are needed to maintain the superconducting state of this kind of cavities. Therefore to maximize the thermal exchange, the superconducting cavities are operated in a liquid or superfluid helium bath. The ability of a certain cavity to retain the RF field with low power dissipation is usually given in terms of the *intrinsic quality factor* (Q_0). The Q_0 is equal to the cavity stored electromagnetic energy multiplied by two times Pi over the amount of energy dissipated in one RF period. TESLA is one of the type of superconducting cavities, which is most frequently used in electron accelerators. This type of resonator has a design resonant frequency of 1.3 GHz, and state-of-the-art TESLA cavities have a Q_0 that exceed $2 \cdot 10^{10}$. To match the cavity with the beam loading and to optimize the RF budget, the required quality factor for operations or *loaded quality factor* (Q_L) is usually lower than the intrinsic one. In low-current SRF CW accelerators based on TESLA cavities a Q_L higher than 10^7 is generally used, that results in a system bandwidth of some tens of Hertz (Padamsee et al. (2008)). Such a narrow bandwidth makes the cavity field very sensitive to disturbances that deforms its geometry in the micron range. These detuning disturbances can originate from the accelerating field radiation pressure, the Lorentz Force Detuning (LFD), and external mechanical disturbances (microphonics). Detuning disturbances make it harder to keep the cavity resonance frequency at a fixed value and have to be compensated. Moreover, when the LFD is comparable to the cavity bandwidth, an instability, the monotonic instability, might cause a loss of gradient if the resonance frequency is not tightly controlled (Schulze (1972)). Therefore, piezoelectric tuners are used when an online correction of the cavity resonance frequency is required. In Section 2, the impact of the monotonic instability on operations is explained and a electromechanical state-space model of a resonant cavity (useful to design a resonance controller) is derived. The parameters used in the model are the ones that are foreseen for the CW upgrade of the European X-Ray Free Electron Laser (EuXFEL), a short pulse superconducting accelera-

tor used to produce high intensity hard X-rays to perform various physical, chemical and biological investigations. In Section 3, the stability conditions of the system, when an integral control on the piezoelectric tuner is applied, are presented. An evaluation of the controller behavior for heavily detuned systems is also presented. In Section 4, the capability of the controller of bringing the system to resonance and preventing the occurrence of the monotonic instability disturbances is evaluated experimentally on multiple TESLA acceleration cavities.

2. CAVITY MODEL

To understand how detuning affects the operation of superconducting cavities, an electro-mechanical model of the cavity has to be derived.

2.1 Electrical model

The following first-order matrix differential equation represents an electrical baseband description of an RF cavity (Schilcher (1998))

$$\dot{\underline{\mathbf{v}}} = \omega_{1/2} \begin{bmatrix} -1 & y \\ -y & -1 \end{bmatrix} \underline{\mathbf{v}} + \begin{bmatrix} \omega_{1/2} \\ 0 \end{bmatrix} V_g, \tag{1}$$

with

$$\underline{\mathbf{v}} = \begin{bmatrix} V_r \\ V_i \end{bmatrix}, \quad |\underline{\mathbf{v}}| = E_{\mathrm{acc}} L, \quad y = 2Q_L \frac{\Delta f}{f_0} \tag{2}$$

Here, V_r and V_i are the in-phase and quadrature part of the cavity accelerating voltage $\underline{\mathbf{v}}$, E_{acc} is the accelerating field, L is the cavity length, y is the detuning factor, f_0 is the design resonant frequency and Δf is the detuning. The generator induced voltage V_g is supposed to be constant and in-phase to simplify the derivations. The detuning factor y can be written as the sum of the cavity predetuning $y_\star$ and the contributions of the cavity mechanical modes driven by LFD or other external forces

$$\begin{aligned} y &= y_\star + \sum_{\mu=1}^{N} y^{(\mu)} = \frac{(2\pi f_0 - \omega_u)}{\omega_{1/2}} + \frac{(\omega_u - \omega_c)}{\omega_{1/2}}, \\ y_\star &= \frac{(2\pi f_0 - \omega_u)}{\omega_{1/2}}, \quad \sum_{\mu=1}^{N} y^{(\mu)} = \frac{(\omega_u - \omega_c)}{\omega_{1/2}}, \end{aligned} \tag{3}$$

with the angular resonant frequency of the cavity ω_c, the resonant frequency of the predetuned cavity at rest ω_u, the cavity half bandwidth $\omega_{1/2}$, and $y^{(\mu)}$ the detuning contribution produced by the mode $\mu \in [1, \ldots, N]$.

2.2 Mechanical model

The mechanical model of the cavity can be represented by a a set of second-order differential equations (Schulze (1972)). Each equation is a particular mechanical mode of the resonator structure:

$$\begin{aligned} \dot{\underline{\mathbf{y}}}^{(\mu)} &= \mathbf{A}_{\mathbf{m}}^{(\mu)} \underline{\mathbf{y}}^{(\mu)} + \mathbf{B}_{\mathbf{m}}^{(\mu)} (u_m^{(\mu)} + K_{lfd}^{(\mu)} |\underline{\mathbf{v}}|^2), \\ \underline{\mathbf{y}}^{(\mu)} &= \begin{bmatrix} y^{(\mu)} \\ \dot{y}^{(\mu)} \end{bmatrix}, \quad \mathbf{A}_{\mathbf{m}}^{(\mu)} = \begin{bmatrix} 0 & 1 \\ -(\omega^{(\mu)})^2 & -\frac{\omega^{(\mu)}}{Q^{(\mu)}} \end{bmatrix}, \\ \mathbf{B}_{\mathbf{m}}^{(\mu)} &= \begin{bmatrix} 0 \\ (\omega^{(\mu)})^2 \end{bmatrix}, \quad K_{\mathrm{lfd}}^{(\mu)} = \frac{2\pi k_{\mathrm{lfd}}^{(\mu)}}{L^2 \omega_{1/2}}. \end{aligned} \tag{4}$$

In the above equation $\omega^{(\mu)}$ is the mechanical mode angular resonant frequency, $Q^{(\mu)}$ is the mode quality factor, $K_{\mathrm{lfd}}^{(\mu)}$ is the normalized LFD constant, $k_{\mathrm{lfd}}^{(\mu)}$ is the LFD constant in $\mathrm{Hz}/(\mathrm{MVm}^{-1})^2$. The input $u_m^{(\mu)}$ represents the time-dependent external mechanical forces produced by microphonics and the fast tuner on the cavity. For SRF cavities $K_{\mathrm{lfd}}^{(\mu)}$ and $k_{\mathrm{lfd}}^{(\mu)}$ are always less than zero because of the Slater's theorem and radiation pressure (Slater (1946); Liepe (2001)). The electrical and mechanical model, (1) and (4), are coupled through the detuning factor y and the squared amplitude of the cavity voltage $|\underline{\mathbf{v}}|^2$.

2.3 Zero-order approximation

A first step towards understanding the effects arising from the coupling of (1) and (4) is to perform a steady-state analysis: the derivative terms are set to zero, whereas the steady-state values are denoted with the zero ("0") subscript. For (1) the following equations are obtained

$$|\underline{\mathbf{v}}_0|^2 = \frac{V_g^2}{1 + y_0^2}, \quad y_0 = -\frac{V_{i0}}{V_{r0}} = -\tan(\theta_0), \tag{5}$$

with θ_0 as the phase angle of the cavity voltage. For the mechanical equations of (4) it results in

$$K_{\mathrm{lfd}} = \sum_{\mu=1}^{N} K_{\mathrm{lfd}}^{(\mu)}, \quad \sum_{\mu=1}^{N} y_0^{(\mu)} = K_{\mathrm{lfd}} |\underline{\mathbf{v}}_0|^2, \tag{6}$$

where K_{lfd} is the total normalized LFD constant of the cavity. Using (5) and (6) with the definition of the detuning parameter in (3) leads to the following equation

$$y_\star = -K_{\mathrm{lfd}} |\underline{\mathbf{v}}_0|^2 \pm \sqrt{\frac{V_g^2}{|\underline{\mathbf{v}}_0|^2} - 1}, \tag{7}$$

and evaluating (7) at resonance ($|\underline{\mathbf{v}}_0| = V_g$, $y_0 = 0$) gives

$$(y_\star)_{\mathrm{res}} = -K_{\mathrm{lfd}} V_g^2, \tag{8}$$

with $(y_\star)_{\mathrm{res}}$ the predetuning that has to be applied to the cavity to achieve the resonance condition.

2.4 Monotonic instability

The result of (8) shows that the steady-state cavity behaviour is driven by the term $K_{\mathrm{lfd}} |V_g|^2$:

case I: $|K_{\mathrm{lfd}} V_g|^2 \ll 1$. The LFD has a low impact and the cavity resonant frequency can be considered independent from the accelerating gradient.

case II: $|K_{\mathrm{lfd}} V_g|^2 \gg 1$. The LFD frequency deviation is higher than the cavity half bandwidth and a variation in cavity gradient produces a sensible variation in the detuning.

In Fig. 1 resonance curves for different values of $K_{\mathrm{lfd}} V_g^2$ are displayed. As it can be seen, above a threshold of $K_{\mathrm{lfd}} V_g^2$ multiple steady-state solutions of the amplitude and phase for a singular value of y appear for (7). Such threshold is $K_{lfd} V_g^2 < -1.54$ and determines the presence of the *monotonic instability* (Schulze (1972)). Due to the presence of the instability, the system may experience significant amplitude and phase jumps if the detuning is changed in a way that a discrete variation of the cavity parameters is required to reach a stable solution of (7) (Fig. 3). One consequence is that if the cavity is driven

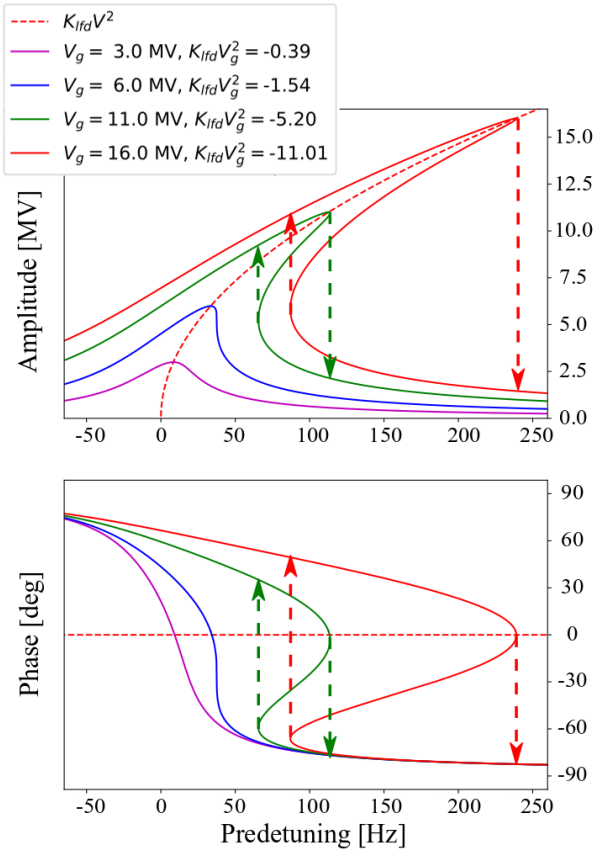

Fig. 1. Static LFD effects on SRF TESLA cavities with $Q_L = 3 \times 10^7$ and the LFD constant $k_{\text{lfd}} = -1\,\text{Hz}/(\text{MVm}^{-1})^2$. For $K_{\text{lfd}}V_g^2 < -1.54$ the cavity is affected by the monotonic instability. Monotonic drop thresholds are indicated by arrows that points downwards. Inverse monotonic drops point upwards.

near resonance, an external disturbance can trigger the instability and make the cavity gradient to incur in a *static drop*. Such an effect is unwanted due to the need to recover the gradient inside the cavity to continue the beam acceleration. A jump in the opposite direction is the *inverse static drop*. For the EuXFEL CW upgrade TESLA cavities have a target design value of k_{lfd} equal to $-1\,\text{Hz}/(\text{MV})^2$, $L = 1.038\,\text{m}$, Q_L higher than $3 \cdot 10^7$ and a maximum E_{acc} of $16\,\text{MV}\,\text{m}^{-1}$. For these parameters it is $K_{lfd}V_g^2 < -11.8$ and the presence of the monotonic instability is expected.

2.5 First order approximation

A way to find out when a monotonic drop happens is to derive a small-signal state-space representation of (1) and (4) and study when the stability conditions are met. In the following, the small gain quantity of a variable x is denoted by δx.
The small-gain representation of (1) is given by

$$\delta\dot{\underline{\mathbf{v}}} = \omega_{1/2}\begin{bmatrix}-1 & y_0\\ -y_0 & -1\end{bmatrix}\delta\underline{\mathbf{v}} - \frac{\omega_{1/2}V_g}{1+y_0^2}\begin{bmatrix}y_0 & 0\\ 1 & 0\end{bmatrix}\sum_{\mu=1}^{N}\delta\underline{\mathbf{y}}^{(\mu)}, \quad (9)$$

and that of (4) by

$$\delta\dot{\underline{\mathbf{y}}}^{(\mu)} = \mathbf{A_m}^{(\mu)}\delta\underline{\mathbf{y}}^{(\mu)} + \mathbf{B_m}^{(\mu)}u^{(\mu)} + \mathbf{G}^{(\mu)}\delta\underline{\mathbf{v}} \quad (10)$$

with

$$\mathbf{G}^{(\mu)} = \frac{2(\omega^{(\mu)})^2K_{\text{lfd}}^{(\mu)}V_g}{1+y_0^2}\begin{bmatrix}0 & 0\\ 1 & -y_0\end{bmatrix}. \quad (11)$$

$\mathbf{G}^{(\mu)}$ is a matrix that couples the field variations to the detuning variations. Then, using (9) and (10), a state transformation is applied to get an amplitude-phase representation with the following transformation matrix

$$\mathbf{T_{ap}} = \begin{bmatrix}\frac{\partial a}{\partial V_r} & \frac{\partial a}{\partial V_i}\\ \frac{\partial\theta}{\partial V_r} & \frac{\partial\theta}{\partial V_i}\end{bmatrix} = \frac{1}{V_g}\begin{bmatrix}1 & -y_0\\ y_0 & 1\end{bmatrix}, \quad (12)$$

such that

$$\begin{bmatrix}\delta a\\ \delta\theta\end{bmatrix} = \mathbf{T_{ap}}\delta\underline{\mathbf{v}}\,, \quad (13)$$

where δa is the amplitude variation normalized to its steady-state value. Using the derived small-signal equations it is possible to write a state-space system in the form

$$\dot{\underline{\mathbf{x}}} = \mathbf{A}\underline{\mathbf{x}} + \mathbf{B}\underline{\mathbf{u}}. \quad (14)$$

The state matrix $\mathbf{A} \in \mathbb{R}^{2(N+1)\times 2(N+1)}$ is defined as

$$\mathbf{A} = \begin{bmatrix}\mathbf{A_e} & \mathbf{H} & \mathbf{H} & \dots & \mathbf{H}\\ \hat{\mathbf{G}}^{(1)} & \mathbf{A_m}^{(1)} & \mathbf{0} & \dots & \mathbf{0}\\ \hat{\mathbf{G}}^{(2)} & \mathbf{0} & \mathbf{A_m}^{(2)} & \ddots & \vdots\\ \vdots & \vdots & \ddots & \ddots & \mathbf{0}\\ \hat{\mathbf{G}}^{(N)} & \mathbf{0} & \dots & \mathbf{0} & \mathbf{A_m}^{(N)}\end{bmatrix}, \quad (15)$$

with

$$\mathbf{A_e} = \omega_{1/2}\begin{bmatrix}-1 & y_0\\ -y_0 & -1\end{bmatrix}, \quad \mathbf{H} = \omega_{1/2}\begin{bmatrix}0 & 0\\ -1 & 0\end{bmatrix}, \quad (16)$$

and

$$\hat{\mathbf{G}}^{(\mu)} = \frac{2(\omega^{(\mu)})^2K_{\text{lfd}}^{(\mu)}V_g^2}{1+y_0^2}\begin{bmatrix}0 & 0\\ 1 & 0\end{bmatrix}. \quad (17)$$

The input matrix $\mathbf{B} \in \mathbb{R}^{2(N+1)\times N}$ is

$$\mathbf{B} = \begin{bmatrix}\mathbf{0} & \mathbf{0} & \dots & \mathbf{0}\\ \mathbf{B_m}^{(1)} & \mathbf{0} & \dots & \mathbf{0}\\ \mathbf{0} & \mathbf{B_m}^{(2)} & \ddots & \vdots\\ \vdots & \ddots & \ddots & \mathbf{0}\\ \mathbf{0} & \dots & \mathbf{0} & \mathbf{B_m}^{(N)}\end{bmatrix}. \quad (18)$$

$\underline{\mathbf{x}} \in \mathbb{R}^{2(N+1)}$ and $\underline{\mathbf{u}} \in \mathbb{R}^N$ represent the state and the input vector, by

$$\underline{\mathbf{x}} = \begin{bmatrix}\delta a\\ \delta\theta\\ \delta\underline{\mathbf{y}}^{(1)}\\ \vdots\\ \delta\underline{\mathbf{y}}^{(N)}\end{bmatrix}, \quad \underline{\mathbf{u}} = \begin{bmatrix}u^{(1)}\\ \vdots\\ u^{(N)}\end{bmatrix}. \quad (19)$$

Measuring $Q^{(\mu)}$ and $k_{\text{lfd}}^{(\mu)}$ for each cavity is not straightforward and instead of relying on a precise model of the cavity, a further assumption is made to simplify the system: the mechanical resonant frequencies are supposed to be at approximately an order of magnitude larger than the resonance half bandwidth of the cavity. Such an assumption is supported by the values reported in literature (Czarski et al. (2006)). Then, for frequencies lower than $\omega_{1/2}$ the derivative terms of the mechanical detuning contributions

$\delta\dot{\mathbf{y}}^{(\mu)}$ can be approximated to zero and the detuning error contributions $\delta\mathbf{y}^{(\mu)}$ can be redefined as

$$\delta\mathbf{y}^{(\mu)} = -\left(\mathbf{A_m}^{(\mu)}\right)^{-1}\left[\hat{\mathbf{G}}^{(\mu)}\underline{\mathbf{x_r}} + \mathbf{B}^{(\mu)}u^{(\mu)}\right] \tag{20}$$

with

$$\underline{\mathbf{x_r}} = \begin{bmatrix}\delta a\\ \delta\theta\end{bmatrix}. \tag{21}$$

As a consequence, (19) can be reduced to a second order system incorporating the terms that depends on K_{lfd} in the electrical part of the system matrix given as

$$\dot{\underline{\mathbf{x}}}_\mathbf{r} = \mathbf{A_e}\underline{\mathbf{x}}_\mathbf{r} - \mathbf{H}\sum_{\mu=1}^{N}\left(\mathbf{A_m}^{(\mu)}\right)^{-1}\left[\hat{\mathbf{G}}^{(\mu)}\mathbf{x_r} + \mathbf{B}^{(\mu)}u^{(\mu)}\right]. \tag{22}$$

With (3), (11) and (16), the reduced system (22) can be defined as

$$\dot{\underline{\mathbf{x}}}_\mathbf{r} = \mathbf{A_r}\mathbf{x_r} + \mathbf{B_r}u_r \tag{23}$$

with

$$\mathbf{A_r} = \mathbf{A_e} - \mathbf{H}\sum_{\mu=1}^{N}\left(\mathbf{A_m}^{(\mu)}\right)^{-1}\hat{\mathbf{G}}^{(\mu)}, \tag{24}$$

$$= \mathbf{A_e} - \omega_{1/2}\frac{2K_{\mathrm{lfd}}V_g^2}{1+y_0^2}\begin{bmatrix}0 & 0\\ 1 & 0\end{bmatrix} \tag{25}$$

and

$$\mathbf{B_r} = \mathbf{H}\sum_{\mu=1}^{N}\left(\mathbf{A_m}^{(\mu)}\right)^{-1}\mathbf{B}^{(\mu)} = \omega_{1/2}\begin{bmatrix}0\\ 1\end{bmatrix}. \tag{26}$$

The term u_r represents the total mechanical perturbation and is defined as

$$u_r = \sum_{\mu=1}^{N}u^{(\mu)} \tag{27}$$

The system in (23) is stable if the eigenvalues of $\mathbf{A_r}$ have a negative real part. This is equivalent to satisfy the following inequality

$$\beta = y_0\left(y_0 + \frac{2K_{\mathrm{lfd}}V_g^2}{1+y_0^2}\right) \geq -1. \tag{28}$$

A stability limit can be found studying (28) near the resonance. In such case a small value of the detuning and a big contribution of LFD is assumed ($|y_0| \ll 1 \ll |2K_{\mathrm{lfd}}V_g^2|$). This simplification leads to the monotonic stability condition

$$y_0 \leq -\frac{1}{2K_{\mathrm{lfd}}V_g^2}. \tag{29}$$

This means that for the EuXFEL CW upgrade, an increase of the detuning of 0.96 Hz can trigger a monotonic drop when driving the cavities at resonance. Therefore, given that such stability can hardly be assured due to pressure drifts, a controller has to be added to prevent the occurrence of monotonic drops.

3. INTEGRAL CONTROL

Using piezo tuners with an integral control policy was already experimentally reported as a successful technique to compensate detuning errors for $Q_L = 1.5\cdot10^7$ (Rybaniec et al. (2017)). Here, we want to theoretically derive stability conditions for such a controller and study its behavior in the presence of a strong monotonic instability. The usage of a pure integral control is justified by the presence of high mechanical resonances $Q(\mu)$ that limit the usage of a proportional controller. For this analysis (23) can be used as a starting point to derive the stability conditions. For the piezo tuners an integral control policy is given by

$$p = p_{t=t_0} + K_I\omega_{1/2}\int_{t_0}^{t}\delta\theta dt\ . \tag{30}$$

In the equation above p the piezoelectric tuner input and K_I the gain of the integrating feedback. The produced mechanical effect on each mechanical mode of the cavity can be described defining $u^{(\mu)}$ as

$$u^{(\mu)} = g^{(\mu)}p + m^{(\mu)}, \tag{31}$$

where $g^{(\mu)}$ is the coupling constant of the mechanical tuner to the mode μ, and $m^{(\mu)}$ is the microphonic contribution. In the following pages, the coupling constant $g^{(\mu)}$ is assumed to be larger than zero. For the model of the cavity system controlled by the feedback the total amount of mechanical coupling g and the total microphonic contribution m have to be taken into account, given as

$$g = \sum_{\mu=1}^{N}g^{(\mu)}, \quad m = \sum_{\mu=1}^{N}m^{(\mu)}. \tag{32}$$

Substituting the integral control law (31) into (27) and then into (23) gives the following closed-loop matrix differential equation

$$\dot{\underline{\mathbf{x}}}_\mathbf{f} = \mathbf{A_f}\underline{\mathbf{x}}_\mathbf{f} + \mathbf{B_f}m \tag{33}$$

$$\tag{34}$$

with

$$\mathbf{A_f} = \omega_{1/2}\begin{bmatrix}-1 & y_0 & 0\\ \beta/y_0 & -1 & g\\ 0 & K_I & 0\end{bmatrix}, \quad \underline{\mathbf{x_f}} = \begin{bmatrix}\delta a\\ \delta\theta\\ p\end{bmatrix}, \tag{35}$$

and

$$\mathbf{B_f} = \omega_{1/2}\begin{bmatrix}0\\ 1\\ 0\end{bmatrix}. \tag{36}$$

The stability of (33) can be derived studying the eigenvalues of the system matrix $\mathbf{A_f}$. Then, given the following assumptions

A.1: the electric source term V_g is constant,

A.2: the dynamics of the cavity is described by (14),

A.3: $\omega_{1/2} \ll \omega^{(\mu)}$,

A.4: the feedback delay is negligible compared to $1/\omega_{1/2}$,

a stability condition can then be expressed by

$$K_I \geq \begin{cases}0 & \text{for} \quad (\beta+1) > 0\\ -2\dfrac{(\beta+1)}{g} & \text{for} \quad (\beta+1) \leq 0\end{cases}. \tag{37}$$

The solution above shows that the system stability is achieved only for positive values of K_I. An attractive property of the closed-loop system is that with a non-zero value of the integrator gain K_I, the system is stable for values of β that are lower than minus one. Therefore, using an appropriate integral gain K_I, it is possible to drive the cavities at otherwise unstable conditions (see (28)).

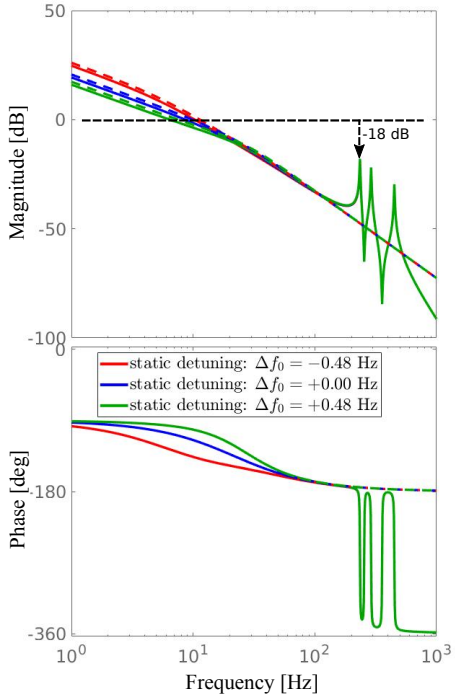

Fig. 2. Loop transfer functions for (14) (continuous lines) and simplified mode-less one (23) (dotted lines). $Q_L = 3 \cdot 10^7$

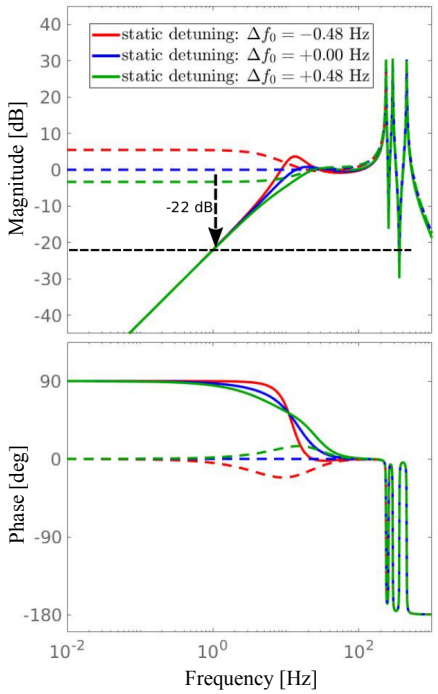

Fig. 3. Comparison between open-loop (dotted lines) and closed-loop (continuous lines) transfer functions from the external mechanical disturbance to the detuning factor y.

Nonetheless, one should keep in mind that the mechanical resonances neglected in the derivation of (33) limit the maximum value of the feedback gain and may make the feedback loop unstable. With the mechanical resonances an additional phase shift of $-180°$ is introduced (4). Thus, to satisfy bode's stability criteria, the integral gain K_I has to be chosen small enough, such that the magnitude of the open loop transfer function is less than one at the eigenfrequency of each mechanical resonance. At the same time, it is desirable to obtain a magnitude of the open loop transfer function as large as possible for frequencies lower than the cavity half bandwidth $\omega_{1/2}$. For the values of Q_L and E_{acc} foreseen in the EuXFEL CW upgrade and using the mechanical values of TESLA cavities listed in Czarski et al. (2006) a good compromise is to set the unit gain on the feedback at values that are approximately one order of magnitude less than the lowest value mechanical eigenfrequency. For $\frac{\omega_{1/2} g K_I}{2\pi} = 10.8\,\text{Hz}$ ($gK_I = 0.5$ for $Q_L = 3 \cdot 10^7$) the maximum magnitude in the open loop transfer function of about $-18\,\text{dB}$ for $y_0 = 0$ at frequencies above 200 Hz (Fig. 2). Such significant gain margin is required to address the uncertainties in the mechanical modes quality factors, couplings, and cavity detuning. At the same time, the closed-loop transfer function shown in Fig. 3 is attenuated by more than $-22\,\text{dB}$ at 1 Hz.

3.1 Considerations over the nonlinear model

All the derivations on the controller stability presented so far use a linearized model of the cavity. A proof of stability on the linearized model is a necessary but not sufficient condition for the stability of the nonlinear model represented by (1) and (4). Furthermore, it has to be tested if the controller can bring the cavity back to a determined setpoint starting from an arbitrary initial detuning value. To do this, the cavity system has to be simulated under the effect of the integral controller. Before, a steady-state analysis is performed, where the time-scale of the controller is assumed to be small compared to the RF timescale of the system. To do this the controller action timescale is supposed to be slow compared to the RF timescale of the system. Such an assumption holds because $|gK_I| < 1$ was chosen. Therefore it is possible to approximate the instantaneous values of cavity status to the steady-state case described by (7) and represented by Fig. 1. Because of this the action of the piezoelectric tuner can be supposed to directly change the zero gradient detuning. Such a study, represented in Fig. 4, shows that the cavity system always returns to the setpoint, independently of the initial detuning condition. If the system starts from the low gradient side of the monotonic instability, first the controller brings it to the high gradient side pushing it through the inverse static drop and then tunes it to the setpoint. In the graphical study, it turns out that the controller brings the cavity back to the phase setpoint independently of the initial detuning even when the system experiences a static drop. A numerical closed-loop simulation of the nonlinear cavity model confirms the behavior derived by the steady-state evaluation and shows that the system converges to the setpoint.

4. EXPERIMENTAL RESULTS

The ability of the designed controller to prevent static drops is verified experimentally on TESLA-type super-

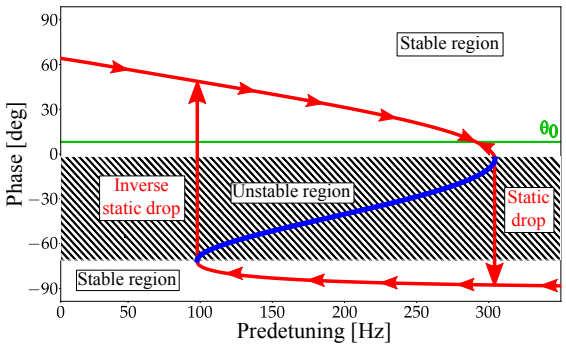

Fig. 4. Trajectory of the cavity phase using the feedback controller. The arrows denote the direction of the trajectory. The red part of the curve constitutes the stable steady-state solutions of (7).

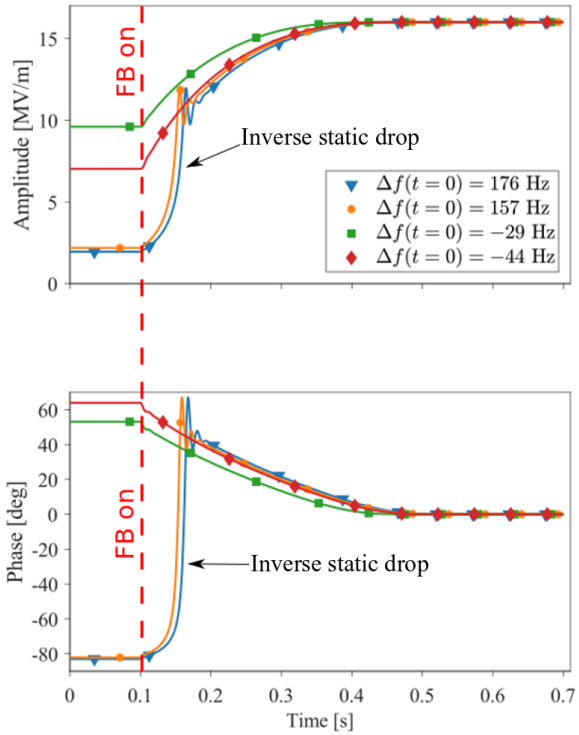

Fig. 5. Simulated closed-loop response of the cavity amplitude and phase with $V_g/L = 16\,\mathrm{MV\,m^{-1}}$ and $Q_L = 3\times10^7$. The complete nonlinear model, constituted by (1) and (4) with mechanical data from Czarski et al. (2006), was used.

conducting cavities. All tests were performed at the Cryo Module Test Bench (CMTB) using a EuXFEL-like cryomodule prototype, XM50.1 (Branlard et al. (2019)) First, the stability of the static detuning is evaluated (Fig. 6). It turned out that every 45 s some event triggers a decrease of the detuning of 4 Hz. This effect originates probably from a subsystem that is used to regulate the helium bath or cavity vacuum. Even though investigations are on-going to determine the cause of such repetitive detuning event, a way to maintain the cavity frequency at a fixed value is helpful to avoid static drops. Then a simultaneous drive of eight cavities in resonance was achieved. An additional Active Noise Controller (ANC) (Rybaniec et al. (2017)) was

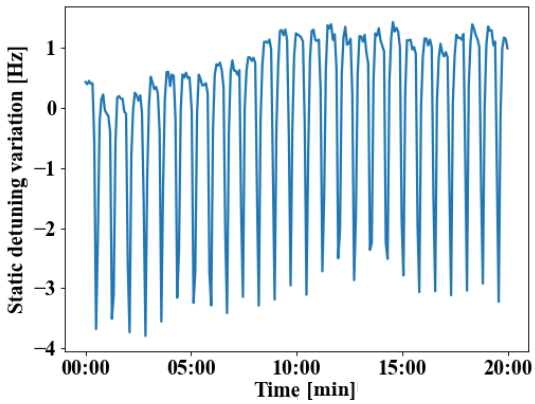

Fig. 6. Measured stability of the static detuning over twenty minutes. A periodic 4 Hz detuning effect is present. The measurement was performed in open loop at $V_g/L = 4\,\mathrm{MV\,m^{-1}}$

used to compensate for repetitive noise with frequencies higher than 1 Hz. The objective was to evaluate how much the monotonic instability impacts the cavity operations at the target gradients of EuXFEL upgrade. All tests were done at $Q_L = 3\cdot10^7$ For gradient values of higher than $10\,\mathrm{MV\,m^{-1}}$ it was hard to achieve good stability or even to reach the cavity resonance without incurring a static drop after some minutes of operation. The severity of the instability effects increased at higher gradients. At gradients around $16\,\mathrm{MV\,m^{-1}}$, the interlock system made the operation of the module impossible due to the large gradient variations correlated to static drops. Successive tests, done with the fast tuner feedback switched on, showed substantial improvement compared to the previous attempts to raise the field inside the cavities to the resonance condition. The controller used in these tests is a CW adaptation of the current EuXFEL LLRF controller, which includes a Proportional-Integral (PI) feedback on the fast tuners. During the tests, only the integral part of the PI controller was used. The unit gain was set to 10.8 Hz as in the simulations. Then, switching on the feedback controller, it was possible to achieve a stable resonance condition on all the cavities inside the module at the same time for gradients up to $16\,\mathrm{MV\,m^{-1}}$. Past studies (Branlard et al. (2018)) confirm the effectiveness of the discussed feedback controller at even higher values of Q_L and E_{acc}. The ability of the controller to bring back the cavity to the desired tune with an arbitrary large initial detuning was also confirmed (Fig. 7). When the system starts from the overtuned case ($\Delta f > 0$, $\theta < 0$), there is an initial delay of about 100 ms which was not seen in the simulations. The reason for this delay could be explained by the presence of backlash in the piezo actuator. Such an effect did not affect the final performance of the feedback controller in keeping the cavity resonance at the desired value.

5. CONCLUSION

In this article, the monotonic instability is studied to see how it would impact the operations of high Q_L SRF cavities driven in CW mode of operation. It is found that such instability would prevent to operate the cavities in stable conditions at high gradients ($> 10\,\mathrm{MV\,m^{-1}}$) because

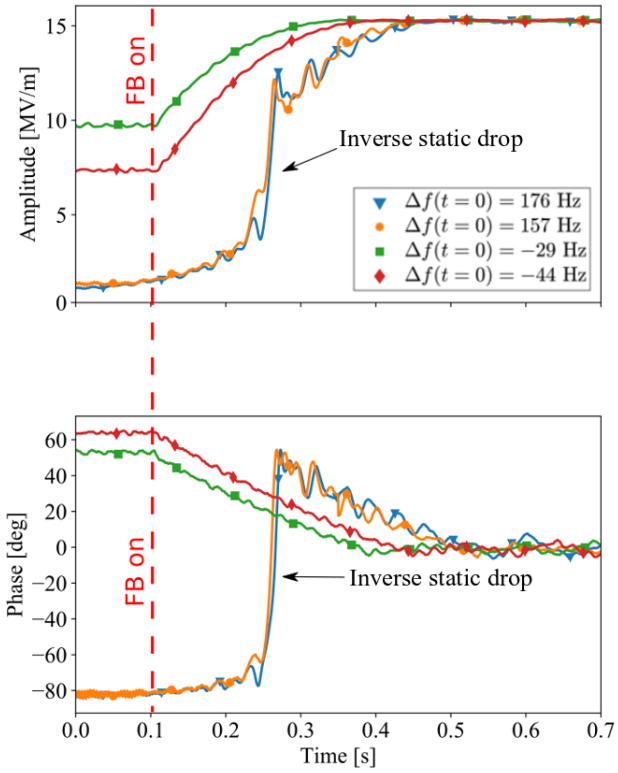

Fig. 7. Experimental closed-loop response of the cavity amplitude and phase with $V_g/L = 16\,\mathrm{MV\,m^{-1}}$ and $Q_L = 3 \times 10^7$. The controller is able to bring the cavity to resonance for either for positive or negative initial value of the detuning.

of the proximity of the RF resonance to the monotonic drop threshold. Therefore, the behaviour of an integral control law of the piezo tuners to mitigate this issue was studied and tested. The analytical explanation why a pure integrating feedback controller on the fast piezoelectric tuner of the cavities is an effective way to prevent monotonic drops was derived theoretically, demonstrated by simulations and verified experimentally. Eight cavities were driven at previously unstable conditions ($E_{\mathrm{acc}} = 13\,\mathrm{MV\,m^{-1}}$, $Q_L = 3 \times 10^7$) thanks to the use of the controller. An added benefit of using the controller derived in this work is the ability to tune the cavities the resonance without the manual intervention of an operator. Some questions remain about the impact of the nonidealities of the piezo actuator (backlash, nonlinearity) and the possible limitations of of the proposed solution. Another aspect to be studied is how drifts in the RF detection chain affect the operations because the fast tuner feedback controller uses the detected RF phase of the cavity signals. Due to changes in humidity and temperature, a variation in the delay of the signals could induce the feedback controller to trip the cavity operating point over the static drop threshold. Finally, the effects that the beam induces on the accelerating field were neglected. Therefore, it has to be studied if more refined detuning estimation techniques are needed rather than relying only on the cavity RF phase to correct the effects produced by LFD. Nevertheless, the electro-mechanical cavity model derived in this paper, and the approach used to correct the monotonic instability can be used as a starting point for further development of the fast tuner feedback controller.

ACKNOWLEDGEMENTS

We would like to thank Dr. J. Sekutowicz, Dr. K. Przygoda, Dr. B. Lautenschlager and M.Sc Ayla Nawaz for the suggestions given on this article. We would like also to thank our colleagues at DESY (groups MSK, MSL, MKS, MCS, MEA and MVS) that made CW tests at CMTB possible.

REFERENCES

Branlard, J. et al. (2018). Highlights of the XM-3 cryomodule tests at DESY. In *Proceedings of LINAC2018*, 388–390. JACOW Publishing, Geneva, Switzerland.

Branlard, J. et al. (2019). Status of cryomodule testing at CMTB for CW R&D. In *Proceedings of SRF 2019*.

Czarski, T., Pozniak, K.T., Romaniuk, R.S., and Simrock, S. (2006). TESLA cavity modeling and digital implementation in FPGA technology for control system development. *Nuclear Instruments and Methods in Physics Research Section A: Accelerators, Spectrometers, Detectors and Associated Equipment*, 556(2), 565–576.

Habs, D. and Köster, U. (2011). Production of medical radioisotopes with high specific activity in photonuclear reactions with γ-beams of high intensity and large brilliance. *Applied Physics B*, 103(2), 501–519.

Liepe, M.U. (2001). Superconducting multicell cavities for linear colliders. Technical report, DESY.

Nakamura, N. et al. (2015). Design Work of the ERL-FEL as the High Intense EUV Light Source. In *Proceedings of ERL 2015*, MOPCTH010.

Padamsee, H., Knobloch, J., Hays, T., et al. (2008). *RF superconductivity for accelerators*, volume 2011. Wiley Online Library.

Raubenheimer, T.O. (2018). The LCLS-II-HE, a high energy upgrade of the LCLS-II. In *Proceedings of FLS2018*, 6–11. JACOW Publishing, Geneva, Switzerland.

Rybaniec, R. et al. (2017). FPGA-based rf and piezocontrollers for SRF cavities in CW mode. *IEEE Transactions on Nuclear Science*, 64(6), 1382–1388.

Schilcher, T. (1998). *Vector sum control of pulsed accelerating fields in Lorentz force detuned superconducting cavities*. Ph.D. thesis.

Schulze, D. (1972). *Ponderomotive stability of RF resonators and resonator control systems*. Ph.D. thesis, Universitt Karlsruhe.

Sekutowicz, J. et al. (2015). Research and development towards duty factor upgrade of the European X-Ray Free Electron Laser linac. *Physical Review Special Topics-Accelerators and Beams*, 18(5).

Serafini, L. et al. (2019). Marix, an advanced mhz-class repetition rate x-ray source for linear regime time-resolved spectroscopy and photon scattering. *Nuclear Instruments and Methods in Physics Research Section A: Accelerators, Spectrometers, Detectors and Associated Equipment*, 930, 167–172.

Slater, J.C. (1946). Microwave electronics. *Reviews of Modern Physics*, 18, 441–512.

Zhu, Z. et al. (2017). SCLF: An 8 GeV cw scrf linac-based x-ray fel facility in shanghai. In *Proceedings of FEL2017*, 20–25. JACOW Publishing, Geneva, Switzerland.